Modeling, System Identification, and Control of ASTREX

N. S. Abhyankar, J. Ramakrishnan, K.W. Byun

Dynacs Engineering Company
34650 U. S. 19N, Suite 301
Palm Harbor, FL 34684

A. Das, Lt. D. F. Cossey, J. Berg

OLAC PL/STS
Edwards AFB, CA 93523-5000

ABSTRACT

The modeling, system identification and controller design aspects of the ASTREX precision space structure are presented in this work. Modeling of ASTREX is performed using NASTRAN, TREETOPS and I-DEAS. The models generated range from simple linear time-invariant models to nonlinear models used for large angle simulations. Identification in both the time and frequency domains are presented. The experimental set up and the results from the identification experiments are included. Finally, controller design for ASTREX is presented. Simulation results using this optimal controller demonstrate the controller performance. Finally the future directions and plans for the facility are addressed.

1 Introduction:

The modeling, system identification and control of the Advanced Space Structures Technology Research Experiments (ASTREX) are the focus of this paper. ASTREX is an evolving test bed situated at the Phillips Laboratory, Edwards AFB, CA. The unique features of the experimental facility include the three-axis large angle slewing maneuver capability and the active tripod members with embedded piezoelectric sensors and actuators. The slewing and vibration control will be achieved with a set of Reaction Control System (RCS) thrusters, a reaction wheel, active members, control moment gyros (CMGs), and linear precision actuators (LPACT). A dedicated control and data acquisition computer is used to command and control this operation. The structure will be fully operational in the near future for implementing the control strategies to maneuver it to achieve retargeting and vibration suppression.

The paper is organized in the three major sections, namely modeling, identification and control. A general description of the testbed is given in the following section.

Description:

The ASTREX structure consists of two major parts; a vertical pedestal (1) 5 meters high supporting the test article (2) through an airbearing system (ABS). The test article is balanced in the floating configuration over the airbearing system by a 180 psi compressed airflow. The central part of the test article, called the hub, is directly connected to the hemispherical ball of ABS. The truss surrounding the hub is constructed by a set of 3" outer diameter graphite epoxy tubes with end fittings and the specially designed 'star nodes'. This primary structure

is connected to the front piece, called secondary, via a tripod made up of composite tubes and consisting of embedded sensors and actuators. The triangular secondary structure supports the reaction wheel and the simulated secondary mirror. A tertiary structure situated behind the primary balances the secondary and houses electronics/ power supply for the data acquisition and control. In addition, a couple of cylindrical masses placed on the sides simulate the trackers. Six sets of triangular plates attached on the front face of the test article simulate a primary mirror. The test article is shown in Figure 1. From its neutral floating configuration, it can undergo ± 20deg roll (local), ± 20deg pitch, and 'unlimited' (± 180deg revolutions) rotation about the vertical axis, limited only by the length of cables and air hoses from the ground.

The RCS thrusters are mounted on the corners of the hexagonal primary structure. Two 8 lb thrusters are placed on the top and bottom nodes for roll control. A set of four 200 lb and 8 lb RCS thrusters are placed near the remaining four corners. Their plate mounts are connected to the primary via truss members. These four thruster units can be rotated on the plate mounts to direct the thrust line by ± 30 deg with respect to the line joining centers of primary and secondary (test article z axis). With the secondary facing 30 deg down, its designed attitude, the thruster line can range between 0 to 60 deg down with respect to the ground. The 500 psi air supply to thrusters is provided by two 30 gallon tanks encased in the hub. The tanks are joined to the thrusters by a set of hoses, ball valves and air filters.

The structure is instrumented with several linear accelerometers which are connected to a set of Butterworth filters. The filtered signals can be acquired remotely by a CDAC unit with a VAX 3100 as a front end computer. It is equipped with Matrixx/ autocode/ real-time-monitor/ system build features to command actuator signals and acquire data from sensors as well as actuators. The computer requires discretized (as against continuous) forms of the control law algorithm for implementation. The CDAC is a parallel processor based system having 32 input and 32 output channel connections for transfer of analog data.

At present, the electronics for the active struts are being installed. Several angular rate sensors will be placed at different locations for line-of-sight error measurements. A set of CMGs and LPACTs will also be positioned on the test article to add slewing and vibration control power to the existing actuators.

2 Modeling:

Over time, the ASTREX structure has grown to be a complicated structure with hundreds of individual parts and bolted joints. An attempt is made to document the distances, dimensions and masses of each component to result in a finite element model (FEM) formatted as a NASTRAN data deck. The input file is grouped into the following components for ease of modification and understanding.

- Pedestal (Figure 2)
- Hub
- Hub-pedestal interface mount
- Primary truss with mirrors and trackers

- Secondary structure
- Tertiary structure and connections
- Tripod (a new component FEM is being developed.)
- Tripod to primary connection/feet plates, etc.
- Thruster mounts and thrusters
- Instruments (mainly concentrated masses)

The complete ASTREX structure is shown in Figure 3. All the above parts are discretized into elements of the types bars, triangular plates, quadrilateral plates, rigid connections and concentrated masses. The grids and their locations are defined in two cartesian coordinate systems: one for the pedestal (x vertically upward, y to the right and z horizontal) and another for the test article (x locally upward, y to the right and z facing secondary). This arrangement leads to a simplified configuration since the test article is allowed to pivot at the top node of the pedestal. The pivot point grid 139 on the primary (primary axes 0.,0.,0.127m) is coincidental with the pedestal origin at grid 501. The pedestal grids are numbered 501 to 599, and the corresponding elements are numbered 401-450 (CBAR) 801-856 (CQUADA4). These numbers have been fixed and it helps in isolating the pedestal model from the test article model for center of gravity/mass balancing checks and implementation on the multibody dynamics software such as TREETOPS. In all there are 537 grids and over 1000 elements including concentrated masses. Masses of individual components are matched with those in the model. All the grids and elements are arranged such as to resemble the structure physically. The inertia properties of the test article are as follows:

Mass = 5091.9 kg,

Center of gravity node: Grid 139

The inertia matrix in x, y, and z local coordinates relative to C.G. location in kg m^2 is

22239.30226 14.63632488 211.0207350
14.63632488 15680.06974 8.164874955
211.0207350 8.164874955 22270.35766

The NASTRAN input file is set up to perform either normal modes analysis (solution 3) or static analysis (solution 1). During the normal modes analysis, the original structural dynamical system is converted into normalized modal formulation: the dynamical equation $M\ddot{\mathrm{x}}+C\dot{\mathrm{x}}+K\mathrm{x}=F$ with M the mass matrix, C the viscous damping matrix, K the stiffness matrix, x the physical degrees of freedom, and F the force vector, becomes $\ddot{\eta}+2\zeta\omega\dot{\eta}+\omega^2\eta = \Phi^T F$ for mass normalization such that $\Phi^T M\Phi$ is an identity matrix. In this equation, η is the modal amplitude vector, ω the diagonal matrix of structural frequencies, Φ the eigenvector matrix, ζ the diagonal matrix of viscous damping factors, and an overdot signifies time differentiation.

The output for solution 3 can be obtained in three formats. The standard output includes eigenvalues, mode shapes, modal element stresses, and restraint forces induced by user supplied or automatically generated point constraints. A constraint check is performed by observing the values of rotational degrees of freedom in eigenvector matrices, providing restraints wherever large values occur and then confirming that the reaction forces produced by these restraints are negligibly small. The standard output is processed by an off-line computer program which uses the eigenvectors, eigenvalues, actuator-sensor information, damping, etc. to generate the control system matrices as a linear time invariant system. In

addition, specifically for ASTREX, the output matrix C for line of sight (LOS) is formulated by combining the optical sensitivity data (provided by Boeing) with various displacements at selected node locations on the primary, secondary and tertiary mirrors. This procedure is used to estimate the mirror motion for each of these three mirrors. The procedure of constructing the output matrix C has been detailed in [1]. The resulting state space model is:

$$\begin{aligned} \dot{x} &= Ax + Bu + Dw \\ y &= Cx \\ z &= Mx + Hu \end{aligned}$$

where A, B, D, C, M, and H are constant matrices and vectors $x, u, y, z,$ and w symbolize states, input, output, measurements, and noise, respectively.

The second output form (output2 module) is generated using the ALTER sequence in NASTRAN for loading into the I-DEAS, Integrated Design and Analysis Software. In the I-DEAS' graphics environment, the model can be viewed and analyzed. This is achieved by selecting appropriate modules and steps in the I-DEAS' menu interactively. The pre-processing analysis and post-processing can all be performed using I-DEAS. For analysis purposes, only the finite element geometry is needed. For viewing the mode shapes in the deformed geometry form or in animation, the mode shapes from NASTRAN output2 are essential. The solution can as well be constructed entirely in the I-DEAS - FEM - Model Solution mode. (For system identification or test correlation, the I-DEAS - TEST module is utilized). In the FE module, the component weights can be evaluated by grouping several different components and evaluating their masses (element-solid properties) according to the assigned groups. As an output, strain energy distribution can also be obtained in the model solution.

The third form of the output (output5 module) is generated using the ALTER sequence for TREETOPS operations. Considering the test article and the pedestal as two individual bodies, separate flex files are generated. In TREETOPS, the problem is set-up as two flexible bodies with two hinges. These id's are the NASTRAN internal id's equivalent to the grid numbers defined by the user. The software allows one to select a different number of modes for bodies by specifying modes retained in the analysis. Upon execution, both the TREEFLX and TREETOPS synthesize multi-bodies as a single structure with pre-assigned degrees of freedom on hinge connections. The single structure with various kinds of sensors, actuators, functions generators, and controllers can be analyzed dynamically for the controlled response, especially during the large angle slew maneuver. (Both linearized and nonlinear formulations are implemented in TREETOPS). An LOS sensor subroutine as well as a controller represented in terms of dynamical matrices can be augmented externally. Other relevant features of TREETOPS include generation of eigenvalues of the combined structure (EIGEN), frequency response function plots, modal cost analysis, and time history of excitations and controlled responses. ASTREX models are generated using the above software.

Modeling is very crucial in quantifying the physical structure. Physical resemblance of the model to the actual structure is just the first step (pretest) in the modeling procedures. Acquiring data during the modal testing and identifying modal parameters of the structure forms the next step. Validation and tuning the structural parameters for model matching are extremely important. With the modeling aspects complete, the system identification of ASTREX is now presented.

3 System Identification:

Model identification in the time domain seeks to solve the inverse problem of deriving a mathematical model that matches, in some sense, the output of a physical system. Identification experiments allow the precise characterization of the physical structure. Some of the parameters obtained from the identification procedures include modal parameters such as frequency, damping ratios and time-domain models such as state space characterizations. For the time domain identification, the q Markov covariance equivalent realization (q COVER) is used which is briefly presented here for the sake of completeness.

3.1 q - COVER Theory:

The objective of the q-Markov COVER identification is to develop state space matrices of a discrete dynamic system given by

$$\hat{x}(k+1) = \hat{A}\hat{x}(k) + \hat{B}u(k), \hat{x}(0) = \hat{x}_0 \quad (1)$$

$$\hat{y}(k) = \hat{C}\hat{x}(k) + \hat{D}u(k) \text{ for } k \geq 0 \quad (2)$$

with input u, output $\hat{y}$, the states $\hat{x}$ and the time sequence parameter k; the state covariance matrix

$$\hat{X} = \lim_{k\to\infty} E\hat{x}(k)\hat{x}^*(k) = \hat{A}\hat{X}\hat{A} + \hat{B}\hat{B}^* \quad (3)$$

is assumed to be positive definite. The infinite pulse response sequence H_i (also called Markov parameters) and corresponding autocorrelation sequence R_i (also called covariance parameters) with i $\rightarrow \infty$ relate to the output data as follows:

$$y(k) = H_0u(k) + H_1u(k-1) + H_2u(k-2) + ... = \sum_{i=0}^{\infty} H_iu(k-i)$$

and

$$R_i = \lim_{k\to\infty} Ey(k+i)y^*(k)$$

The system in eq. 1, along with the positive definite assumption on the state covariance, is said to be a q-Markov COVER of the system generating the above infinite data sequences, if the first q and q-1 terms of $\{H_i\}_0^\infty$ and $\{R_i\}_0^\infty$ are equal to those of the finite data sequences $\{\hat{H}_i\}_0^q$ and $\{\hat{R}_i\}_0^{q-1}$. Both sequences $\hat{H}_i$ and $\hat{R}_i$ can be expressed in terms of matrices $(\hat{A}, \hat{B}, \hat{C}, \hat{D})$. The quadruple $(\hat{A}, \hat{B}, \hat{C}, \hat{D})$ is extracted in an inverse manner from the experimental data obtained by exciting the structure by a finite series of pulses. The realization problem, finding all minimal stable q-Markov COVERs given $\{\hat{H}_i\}_0^q$ and $\{\hat{R}_i\}_0^{q-1}$, is based on the factorization and projection of two data matrices $\mathbf{D_q}$ and $\bar{\mathbf{D}}_\mathbf{q}$(functions of a finite number of Markov and Autocorrelation parameters) obtained from the pulse response data:

$$\mathbf{D}_q \triangleq \mathbf{R}_q - \mathbf{H}_q\mathbf{H}_q^*$$

$$\bar{\mathbf{D}}_q \triangleq \mathbf{R}_q - \bar{\mathbf{H}}_q\bar{\mathbf{H}}_q^* \quad (4)$$

The interested reader is directed to references [2,3] for more details and proofs. The data acquisition procedure in the ASTREX lab for conducting the identification experiments is now presented.

3.2 Data acquisition:

The data required for the system identification has been obtained from accelerometers and selected RCS thrusters (8-lb) through a control and data acquisition computer. A block diagram, given in Figure 4, describes the acquisition process. The locations for accelerometers are carefully selected based on expectations of capturing all the relevant structural modes. These accelerometers and thruster pin-outs are connected to a coaxial junction box situated on the tertiary structure. Signals from the accelerometers, powered by a constant current amplifier, are filtered and amplified prior to acquisition with the help of a set of 8^{th} order Butterworth filters having a 200 Hz bandwidth and the capability to amplify signals 34 times maximum. The data acquisition is monitored through a parallel processor CDAC having a VAX3100 as the front end computer. CDAC is also linked to the ABS computer to transfer information from gimbals, LVDTs, and encoders connected to ABS. The sampled data is saved in the ASCII format specifically to transport to other software such as MATRIXX, I-DEAS TEST, etc. to perform system identification. The identification of a large structure such as ASTREX is best performed using the techniques suitable for multi-input multi-output systems. The application of the q-Markov COVariance Equivalent Realization (COVER) algorithm to ASTREX is now presented.

3.3 Identification of ASTREX:

Markov and autocorrelation parameters of the system to be identified are determined from the experimental data. There are two approaches to this problem:

(i) Excite the system by a pulse input to obtain the Markov parameters and by a white noise input to obtain the autocorrelation factors.

(ii) Obtain both the Markov and autocorrelation parameters from the pulse response.

The second approach is used in this work since one experiment yields both the Markov and autocorrelation data.

Identification experiments were conducted on the ASTREX test article in August 1991. The compressed air thruster developed by Boeing was used in the experiments. The details of the identification experiment and the results are described as follows.

The actuators used in system identification were the 8 lb bidirectional thrusters. The thrusters are designed to operate using compressed air at 500 psi. At the time of testing, however, a 150 psi compressor was used to provide the compressed air (a new 500 psi compressor is now fully operational). Additionally, there was a pressure drop to 70 psi across the air filters. Based on this pressure and the thruster operation mode (blow down) a thrust of about 3 lbs was achieved. The input voltage versus thrust command of the actuator was linear. The tank pressure changed from 150 psi to a 100 psi during this test. The identification tests were conducted using 4 millisecond pulses with a 2 second data sampling time per experiment.

3.4 Identification at 250 Hz:

Four actuators and thirty-one sensors were used in the identification experiment. The actuators were located on the primary truss. The sensor locations and their identification numbers are shown in Table 1. Piezoelectric accelerometers with limits ± 5 g were used as sensors in this experiment. Channel 1 of the CDAC was used to record the input voltage from the thrusters, while channels 2-32 were used to record the accelerometer outputs. Since the pulse was of a low magnitude and short duration (4 ms), the gain on the Butterworth filters was set to 34. This resulted in a significantly better signal-to-noise ratio ($\simeq 8$). The noise in the outputs were essentially downstream of the Butterworth filter. The q-Markov covariance equivalent realization technique with pulse inputs was used in the identification work. The pulse input is applied one-at-a-time at each actuator location. For consistency in measurement, each experiment was repeated 10 times. At the first actuator location, the pulse was applied 10 times, at 2 second intervals. This was repeated at the other three locations and the raw data files were obtained.

The data collection and processing procedure is shown in Figure 5. For the first identification run, the data from experiment one was averaged and detrended. Then the q-COVER algorithm was applied to the six outputs given in Table 2 for 50^{th} order Markov COVER. The applied pulse amplitudes to thrusters are: [0.9122, 0.9246, 0.8903, 0.908]. The intensities are the square of these amplitudes. From the singular value plot of the matrix $\mathbf{D}_q$, a 50^{th} order state space realization is derived. Figures 6 and 7 show the correlation between the time responses of the identified data from channels 2 and 5 versus the lab time history data. The FFT for these output channels is shown in Figure 8 (Solid line represents LAB data dashed line represents IDM response). The eigenvalues in the 10-30 Hz range for the identified model are given in Table 3. A frequency response function was also generated between 0-50 Hz using a tripod accelerometer and the first actuator. The results from the time domain identification are close to the frequency domain results.

3.5 Frequency Response Function:

It is well known that a system's transfer function corresponding to any input/output pair can be represented graphically in the Laplace plane by plotting the system's complex poles and zeros. The poles of a second order viscously damped system are intimately related to the modal natural frequencies and modal damping ratios. Therefore the knowledge of a system's poles is sufficient for the identification of the modal parameters. In order to determine all the poles of interest, one has to investigate multiple sets of input/output pairs. The frequency response function (FRF) is the ratio of the output to the input of a system with respect to the frequency of excitation.

A single-input single-output (SISO) transfer function measurement between two locations on ASTREX was performed using the HP3562A dual channel analyzer. The structure was excited by a shaker at the left-top node on the shaker in the horizontal direction (z global). A force transducer situated between the shaker and the structure provides the analog input source level. A collocated accelerometer record was used to obtain a frequency response function (FRF) shown in Figure 9. This is the latest FRF of the structure after the new TRW active struts were installed. The frequencies 10.25 and 10.625 are classified to be bending in the yz and xz planes, respectively. Large numbers of such FRFs will be needed to identify the frequencies, mode shapes, and damping accurately. This FRF of the present ASTREX configuration provides one with a modal survey of the test article.

4 Control:

Control design procedure and results with related methods are presented in this section. The procedure shown in Figure 10 can be represented by the following steps: frequency weighting on LOS outputs, model reduction using Modal Cost Analysis(MCA), and reduced-order controller design using Output Variance Control (OVC). Now the OVC and MCA methods are discussed. Their applications can be found in [5,6].

4.1 OVC Theory:

The objective of the OVC problem is to design a controller that minimizes input energy subject to inequality constraints on the output variances. From the application standpoint, only the discrete form of the OVC theory is presented here.

Consider the following time-invariant, stabilizable and detectable continuous system state space model:

$$\begin{aligned} \dot{x}_p &= A_p x_p + B_p u + D_p w_p \\ y &= C_p x_p \\ z &= M_p x_p + v_p \end{aligned} \tag{5}$$

where $x_p \in R^{n_x}$, $y \in R^{n_y}$, $z \in R^{n_z}$, and $u \in R^{n_u}$ are the state, output, measurement and control vectors, respectively. The disturbance vector $w \in R^{n_w}$ is a zero mean white noise process with intensity $E\left\{w_p(t)w_p^*(\tau)\right\} = W_p\delta(t-\tau)$ while the measurement noise v_p has an intensity $V_p\delta(t-\tau)$. The objective is to design an full order controller

$$\begin{aligned} u &= Gx_c \\ \dot{x}_c &= A_c x_c + Fz \end{aligned} \tag{6}$$

which minimizes the control energy

$$J = E_\infty(u^T R u) = tr\ RGX_cG^T\ , \tag{7}$$

where $X_c = E_\infty x_c x_c^T$ is the controller variance, subject to equations 5 and 6 and satisfies the output variance inequality constraints

$$E_\infty\ y_i^2(t) \le \sigma_i^2 \quad i = 1, 2, \ldots, n_y \tag{8}$$

Defining a new state vector x as $x = \left[(x_p - x_c)^T \quad x_c^T\right]^T$, equations 5 and 6 can be written as

$$\dot{x} = Ax + Dw \tag{9}$$

$$y = Cx \tag{10}$$

where

$$A = \begin{bmatrix} A_p - FM_p & A_p - FM_p + B_pG - A_c \\ FM_p & A_c + FM_p \end{bmatrix}$$

$$D = \begin{bmatrix} D_p & -F \\ O & F \end{bmatrix},\quad C = [C_p\ C_p],\quad u = [0\ \ G]\,x,\quad w = \begin{bmatrix} w_p \\ v_p \end{bmatrix} \tag{11}$$

The state covariance matrix of the system (9) becomes

$$X \triangleq E_\infty(xx^*) = \begin{bmatrix} P & X_{12} \\ X_{12}^T & X_c \end{bmatrix} \tag{12}$$

and the state covariance of the plant (5) becomes $X_p = P + X_c$, where P is the error covariance matrix and

$$W = \begin{bmatrix} W_p & 0 \\ 0 & V_p \end{bmatrix} \tag{13}$$

The OVC problem is expressed as an equivalent nonlinear programming problem in which an augmented objective function is minimized. The inequality variance constraint in the necessary conditions is handled via Kuhn-Tucker conditions. The solution of the necessary conditions results in the following algorithm for a discrete system.

4.2 OVC Algorithm for the Discrete System:

Given data $\{A_p, B_p, C_p, D_p, M_p, W_p, V_p, Q_o, R, \sigma_i, \epsilon_i, n\}$

where $Q_o > 0$ is a diagonal matrix

Step 1: Compute the Filter gains F through Riccati solution P by satisfying

$$\begin{aligned} 0 &= A_pPA_p^T - P - A_pPM_p^T(V_p + M_pPM_p^T)^{-1}M_pPA_p^T + D_pW_pD_p^T \\ F &= A_pPM_p^T(V_p + M_pPM_p^T)^{-1} \end{aligned} \tag{14}$$

Step 2: Compute the maximal accuracy solution

$$y_i^2 \text{ (Max. Accuracy)} = \left[C_pPC_p^T\right]_{ii} \tag{15}$$

Computation is terminated if $\sigma_i^2 < [C_pPC_p^T]_{ii}$ for any i.

Step 3: Compute the controller gain matrix G through Riccati solution $\tilde{K}$

$$\begin{aligned} 0 &= A_p^T\tilde{K}A_p - \tilde{K} - A_p^T\tilde{K}B_p(R + B_p^TKB_p)^{-1}B_p^T\tilde{K}A_p + Q_k \\ G &= -(R + B_p^TKB_p)^{-1}B_p^T\tilde{K}A_p \end{aligned} \tag{16}$$

Solve the controller covariance equation

$$0 = (A + BG)X_c(A + BG)^T - X_c + F(V + M_pPM_p^T)F^T \tag{17}$$

Compute the output variance

$$(y_{i_{RMS}})^2 = [C_p(P + X_c)C_p^T]_{ii} = [C_pX_pC_p^T]_{ii} \tag{18}$$

Step 4: Verify the convergence condition

$$[y^2_{i_{RMS}} - \sigma_i^2]Q_{ii} \leq \epsilon_i \text{ for all } i \text{ STOP}$$

OR update Q_k as $Q_{k+1} = [\ \frac{y^2_{i_{RMS}}}{\sigma_i^2}\ ]^n Q_k$ and return to step 3.

The necessary condition for the OVC problem is the same as that of the LQ class of problems with some diagonal output weighting matrix that is iteratively updated. From the above equation, it turns out that if $E_\infty y_\alpha^2(t) < \sigma_\alpha^2$, then the corresponding weighting q_α approaches 0. Physically this means that this particular output $y_\alpha(t)$ is not critical to the design and the constraint $T_\alpha \leq \sigma_\alpha^2$ is not necessary. It is, of course, not known *a priori* which constraints will be binding, and so all constraints must be stated in the problem. More details on the OVC method can be found in reference [9]. While there is no convergence proof for the algorithm, experience shows that the algorithm will converge if the tuning parameter n is sufficiently small.

4.3 Modal Cost Analysis (MCA):

The evaluation model is reduced to Riccati solvable dimensions by the MCA method. The reduced order model is called the design model. The controller is designed based on this model. The contribution of the mode i to the scalar cost function is called "modal cost." Modes are truncated such that the design model retains a percentage of the cost of the evaluation model.

Consider the system in modal coordinates

$$\begin{aligned} \dot{\eta}_i &= \lambda_i \eta_i + b_i^* u \qquad i = 1, \ldots, n_x \\ y &= \sum_{i=1}^{n_x} C_i \eta_i \qquad \eta_i(0) = 0 \end{aligned}$$

with the scalar cost function

$$V = \sum_{\alpha}^{n_u} \int_o^\infty y^{\alpha^*}(t) Q y^\alpha(t) dt$$

where $y^\alpha(t)$ is the response to $u_\alpha(t) = \mu_\alpha \delta(t)$. For the modal coordinate η_i, the modal cost is given by

$$V_{\eta_i} = [X_m\ C_m^*\ Q\ C_m]$$

where

$$\begin{aligned} 0 &= X_m A_m^* + A_m X_m + B_m \mathcal{U} B_m^* \\ \mathcal{U} &= diag \begin{bmatrix} \mu_1^2 & & \\ & \ddots & \\ & & \mu_{nu}^2 \end{bmatrix} \end{aligned}$$

and $A_m = diag\,[\ldots \lambda_i \ldots]$ with B_m and C_m being corresponding modal input/output coefficient matrices. From the computational viewpoint, closed form solutions of the Lyapunov

equation in modal coordinates are used. Furthermore, some of the calculations are carried out in the real Jordan form coordinates yielding the appropriate design model.

The controller design iterations use the integrated MCA-OVC formulation. The design model determined by the MCA approach depends on the output weighting matrix Q, which reflects the importance of each output. The OVC approach iteratively determines the Q matrix that yields a controller satisfying output inequality constraints. Thus the model reduction procedure is influenced by the designed controller. The integrated procedure is implemented as follows. Based on an initial weighting matrix, Q_o, the MCA approach is used to design a reduced-order model which is followed by the OVC loop. The OVC loop yields a new Q matrix. This matrix Q is now used in the MCA procedure to design a new reduced order model. Controller design is repeated until the reduced-order model ceases to change.

4.4 Design Results:

An 82^{nd}-order finite element model, with a 4 msec sample period, is used as the ASTREX model. Eight accelerometers and ten RCS jets are mounted on the test article; four 200-lb jets are primarily used for slews, four 8-lb jets are used for vibration control, and two 8-lb jets coupled to each other control roll motion. The RCS jets are assumed to have first-order lags with their corner frequencies at 30 Hz, while the accelerometers are assumed to have high bandwidth. Thus the order of the composite system (also the evaluation model) consisting of ASTREX, actuator, and sensor dynamics is 91.

For vibration suppression study, only the six 8-lb jet locations are used as control input channels, while all the jet locations are considered as disturbance input channels. The noise intensity matrices W and V for actuator and sensor noises are defined as

$$W = \text{diag } [2.02,\ 2.02,\ 2.02,\ 2.02,\ 2.02,\ 1260,\ 1260,\ 1260,\ 1260]\ N^2$$
$$V = \text{diag } [1.0,\ 1.0,\ 1.0,\ 1.0,\ 1.0,\ 1.0,\ 1.0,\ 1.0] \times 10^{-6}\ g^2$$

where g is the gravity acceleration constant. The output y to be controlled consists of the x and y components of the LOS outputs in the primary ($losP$), secondary $x_(losS$), tertiary ($losT$) mirrors, and the average of the three (los):

$$y^T = [x_{losP},\ x_{losS},\ x_{losT},\ x_{los},\ y_{losP},\ y_{losS},\ y_{losT},\ y_{los}]$$

The reduced-order controller is sought in discrete time domain for ease of implementation on the CDAC. A 24^{th} order controller is designed based on the MCA-OVC algorithm such that the LOS output and control variances are minimized. As shown in Figure 10, the LOS outputs are weighted using a frequency-dependent function accounting for the actuator dynamics and also the control bandwidth. Also, unfavorable frequency components, such as the pedestal vibration modes, are directly augmented in the controlled output matrix along with the LOS outputs. Then the iterative use of the MCA and OVC algorithms tune the performance of the closed-loop system.

The controller is evaluated on the 91^{st}-order evaluation model. The open-loop variances of the composite system are given by

$$[9.0,\ 16.6,\ 0.013,\ 16.9,\ 3.6,\ 9.9,\ 0.010,\ 11.8]\ \text{arcsec}^2$$

The LOS output variances realized by the controller are

$$[6.7,\ 9.1,\ 0.010,\ 10.3,\ 2.5,\ 5.9,\ 0.010,\ 7.2]\ \text{arcsec}^2$$

The control variances are also listed as follows:

$$[10.7,\ 20.2,\ 15.4,\ 13.4,\ 26.0]\ \text{N}^2$$

Figure 11 shows the time response plot of typical outputs. The secondary mirror LOS outputs achieve moderate reductions in the output variances with low control input variances. The frequency components at 3 to 5 Hz, appearing in the primary mirror LOS outputs, are due to pedestal structure vibration, and require larger control effort for suppression. The controller designed for vibration suppression can now be implemented on ASTREX. Although implementation is beyond the scope of this paper, the procedure is presented nevertheless for the sake of completeness.

4.5 Implementation:

The CDAC has the software MATRIX$_X$, Autocode, and System_build which generate signals for actuators, and acquire data. The operation is performed by building block diagrams to process data in either continuous or discrete system form. For implementation, however, only the discretized control gain matrix form can be used, and thus the controller should be designed in a discretized version. The control 'superblock' basically relates sensor inputs to the actuator inputs, and depends on the method of controller design. For ASTREX, the encoder data converted in terms of quaternions or Euler angles, mainly for slewing, together with measurements of LOS error/accelerometers for vibration suppression can form the sensor data. At present, the control signals are of thrusters (14 total) and for reaction wheel (1). Monitoring of the control process is done in the interactive animation software. It is also to be noted that, due to their interactive nature, both the slewing and vibration must be controlled simultaneously. In other words, for ASTREX, both motions cannot be isolated from one another.

5 Plan:

The following items are currently in the planning stage.

- Component FEM for the tripod active struts.
- Evaluation of dynamic characteristics of thrusters (14) and reaction wheel.
- Acquisition, installation, and testing of LOS sensors.
- A detailed modal survey.
- Model updates based on the experimental data.
- Closed-loop vibration and slewing control.

6 Concluding Remarks

The modeling, identification and controller simulation aspects of the ASTREX testbed are presented in this paper. A precision space structure such as ASTREX provides the structural dynamics and control community with a testbed in which to test and implement emerging technologies. With the establishment of the baseline identification procedures, future updates to ASTREX can be easily handled. A comprehensive look at the modeling, identification and some controller synthesis approaches to ASTREX have been presented. With the structural/hardware development complete, future directions include large closed loop slewing experiments on ASTREX.

7 References

1. *Updated ASTREX State Space Model*, Dynacs Eng. Co., Oct. 90.

2. A.M. King, U.B. Desai and R.E. Skelton, *A Generalized Approach to q-Markov Covariance Equivalent Realizations for Discrete Systems,* 1987 American Control Conference, Minneapolis, MN.

3. U.B. Desai and R.E. Skelton, *Partially Nested q-Markov Covariance Equivalent Realizations,* CTAT, Vol. 3, No. 4, pp. 323-342, December 1987.

4. C. Hsieh, R.E. Skelton and F.M. Damra, *Minimum Energy Controllers with Inequality Constraints on Output Variance*, Opt. Control Appl. & Methods, vol. 10, pp. 347-366, 1989.

5. J. Ramakrishnan, K.W. Byun, R. Skelton, and Lt. D.F. Cossey, *ASTREX Controller Design: OVC and OCC Approach*, NASA-DOD Conference, Orlando, FL, pp. 202-213, Nov. 1990.

6. A. Hu, R.E. Skelton, G.A. Norris and D.F. Cossey, *Selection of Sensors and Actuators with Applications to the ASTREX Facility*, Proceedings of the 4th NASA/DoD CSI Conference, Orlando, FL, Nov. 1990.

Table 1: ASTREX Sensor Locations

CDAC Channel	ASTREX Node #	Sensor Connector #	x	y	z	Comments
1	Thruster				√	
2	197	56		√		Tripod Upper
3	218	43	√			Secondary Backface
4	195	60		√		Tripod Left
5	206	58		√		Tripod Upper
6	196	64		√		Tripod Right
7	204	61	√			Tripod Left
8	196	63	√			Tripod Right
9	197	55	√			Tripod Upper
10	205	65	√			Tripod Right
11	195	59	√			Tripod Left
12	218	44		√		Secondary
13	204	62		√		Tripod Left
14	204	70			√	Tripod Left
15	247	21			√	Primary
16	197	67			√	Tripod Upper
17	196	71			√	Tripod Right
18	206	68			√	Tripod Upper
19	205	72			√	Tripod Right
20	15	51	√			Tertiary
21	223	45		√		Secondary
22	250	26	√			Primary
23	195	69			√	Tripod Left
24	205	66		√		Tripod Right
25	233	33			√	Primary
26	244	4		√		Primary
27	238	16		√		Primary
28	245	22		√		Primary
29	241	11			√	Primary
30	26	54			√	Tertiary
31	1	52		√		Tertiary
32	206	57	√			Tripod Upper

Table 2: Identification Input Channels

Output #	Channel #	Location
1	2	Tripod
2	5	Tripod
3	7	Tripod
4	10	Tripod
5	11	Tripod
6	12	Secondary Plane

Table 3: ID Model Eigenvalues

ω(Hz)	ζ
10.2	0.8578
13.662	0.0226
14.3	0.1072
18.713	0.0243
19.24	0.0253
23.13	0.0334
27.22	0.0066
28.72	0.0104

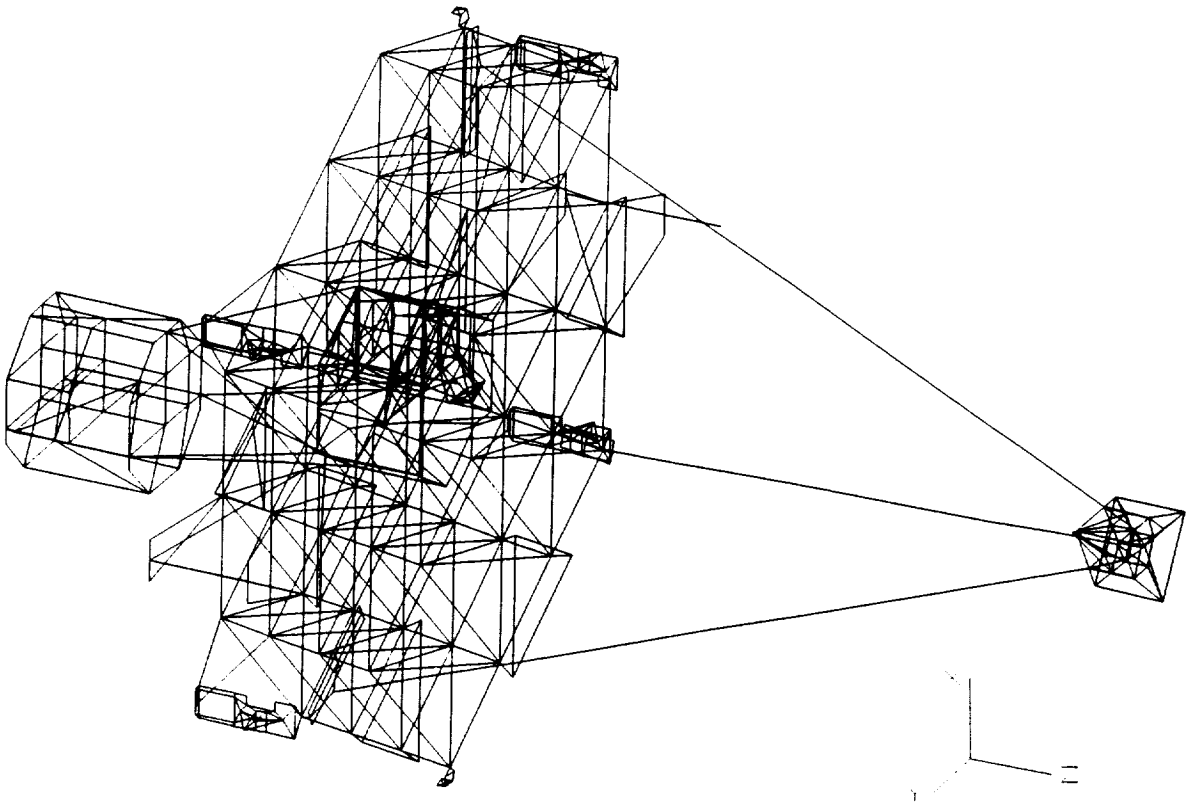

Figure 1: Test article substructure.

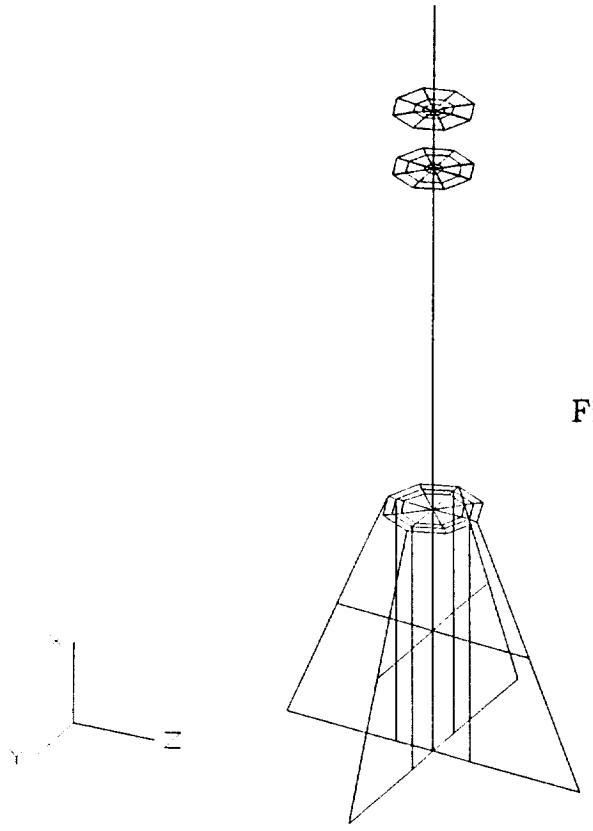

Figure 2: Pedestal substructure.

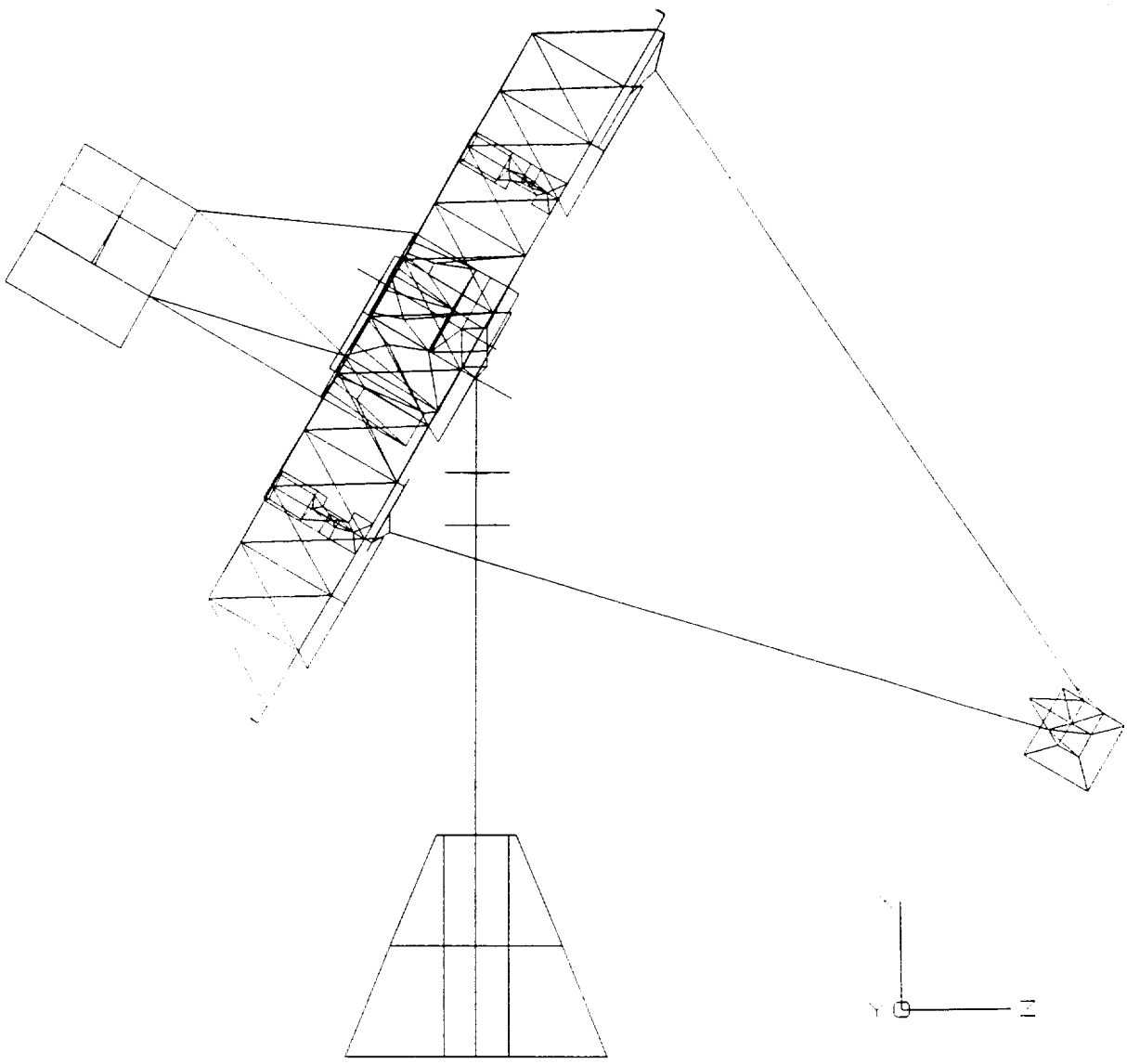

Figure 3: Complete ASTREX structure.

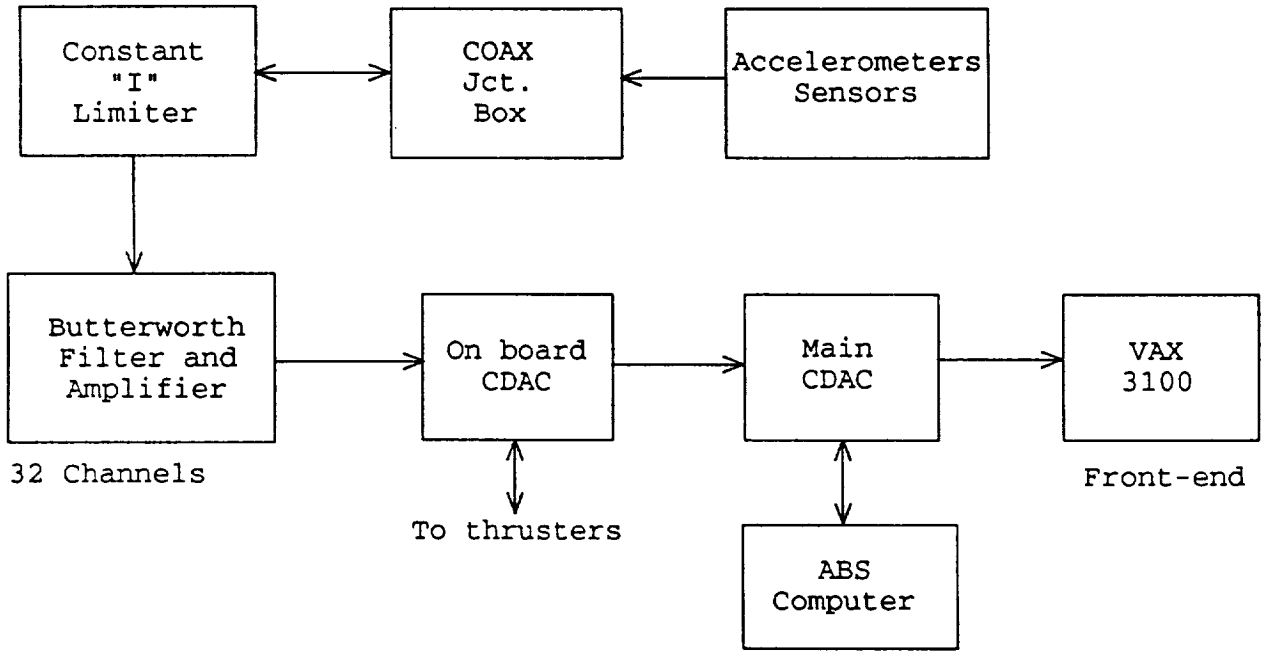

Figure 4: Data acquisition process.

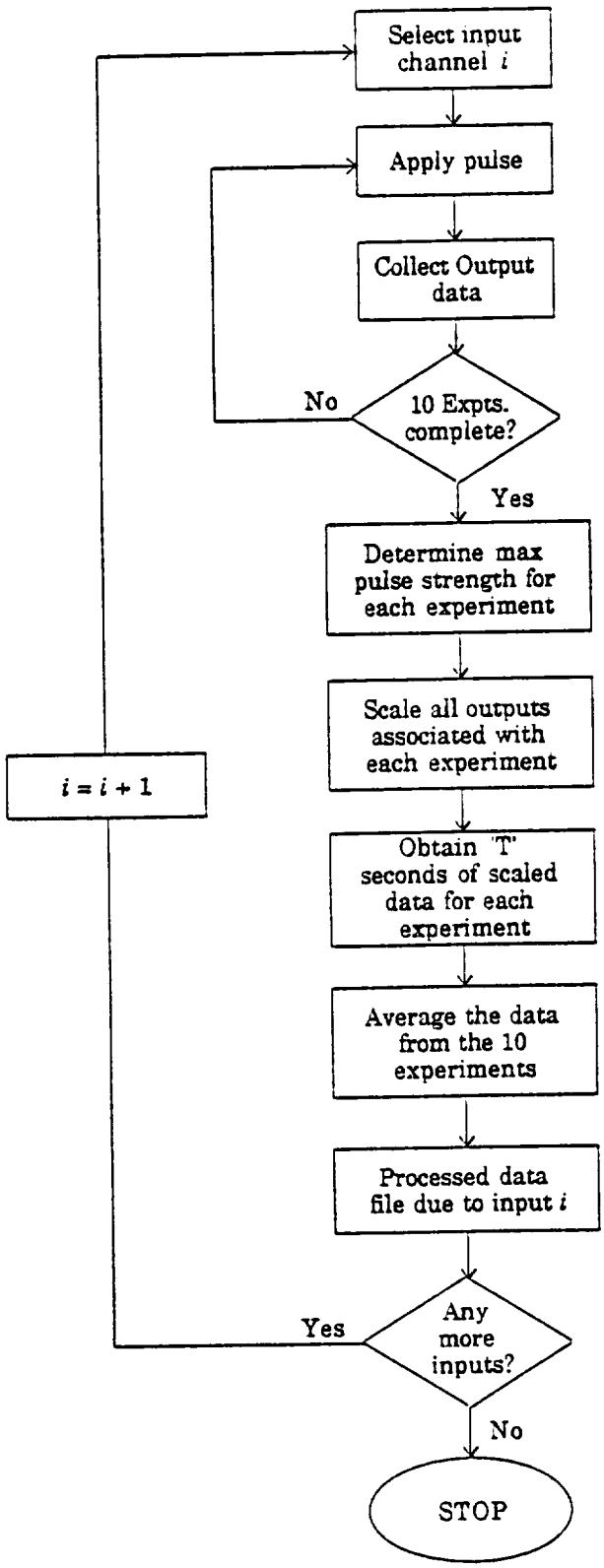

Figure 5: Data collection and processing procedure.

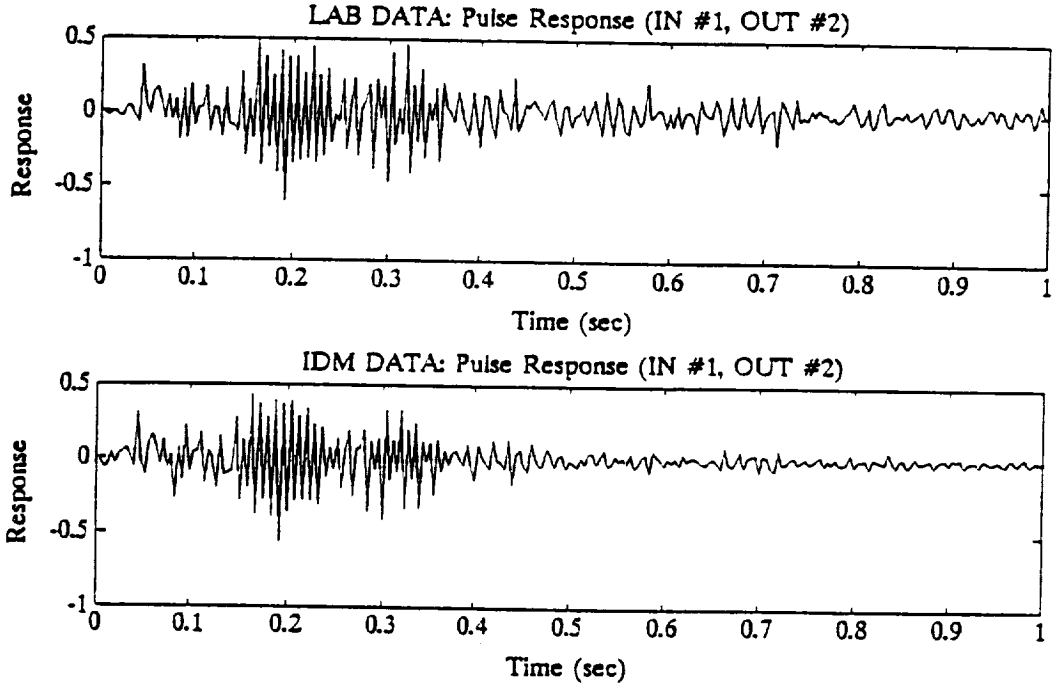

Figure 6: Pulse response: lab data vs. IDM (Identified) data, channel 2.

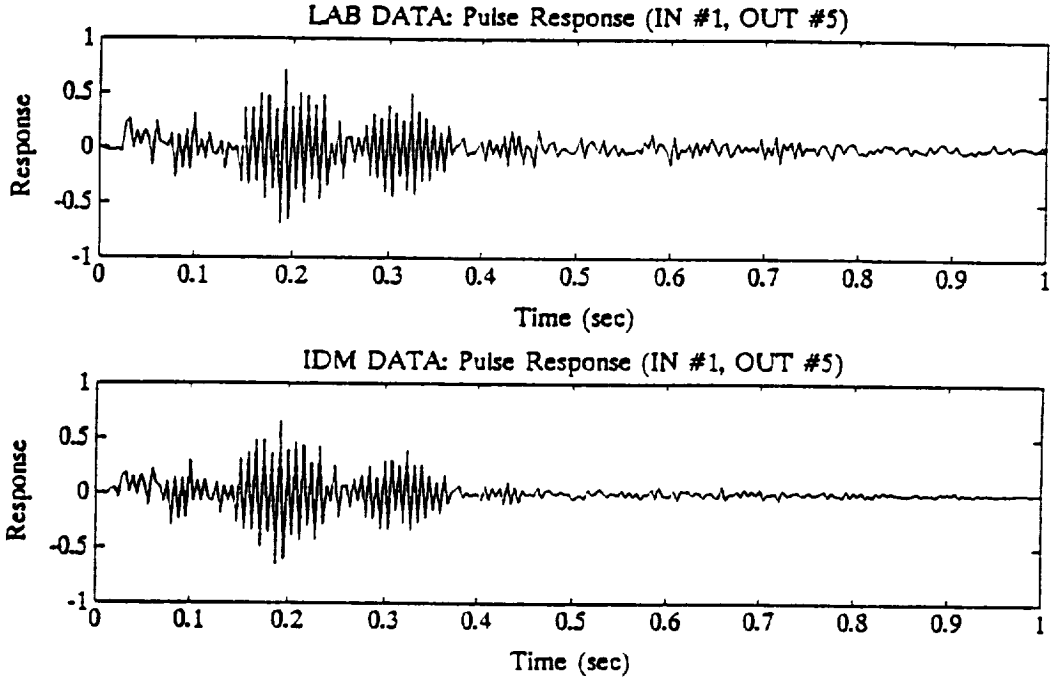

Figure 7: Pulse response: lab data vs. IDM (Identified) data, channel 5.

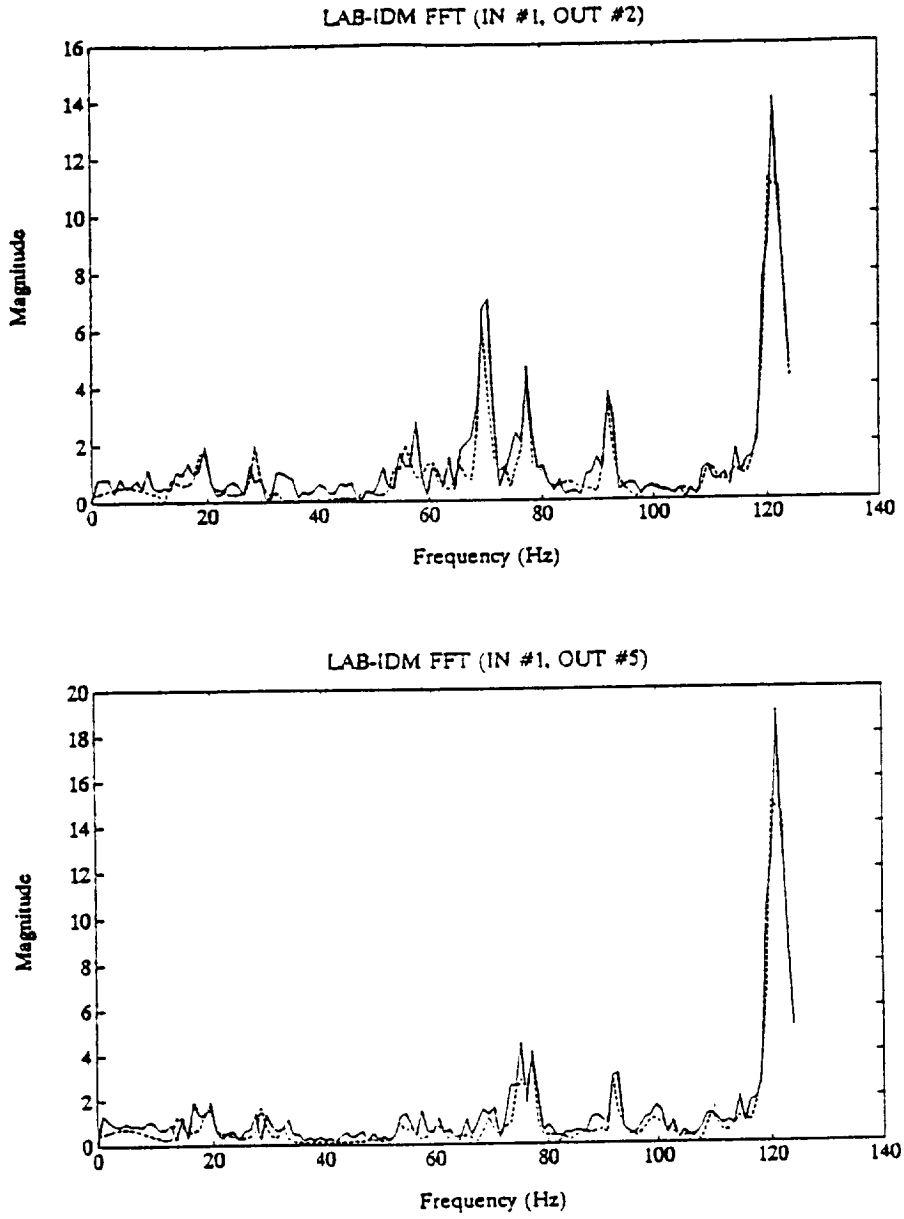

Figure 8: Frequency response: lab data vs. IDM (Identified) data, channels 2 and 5.

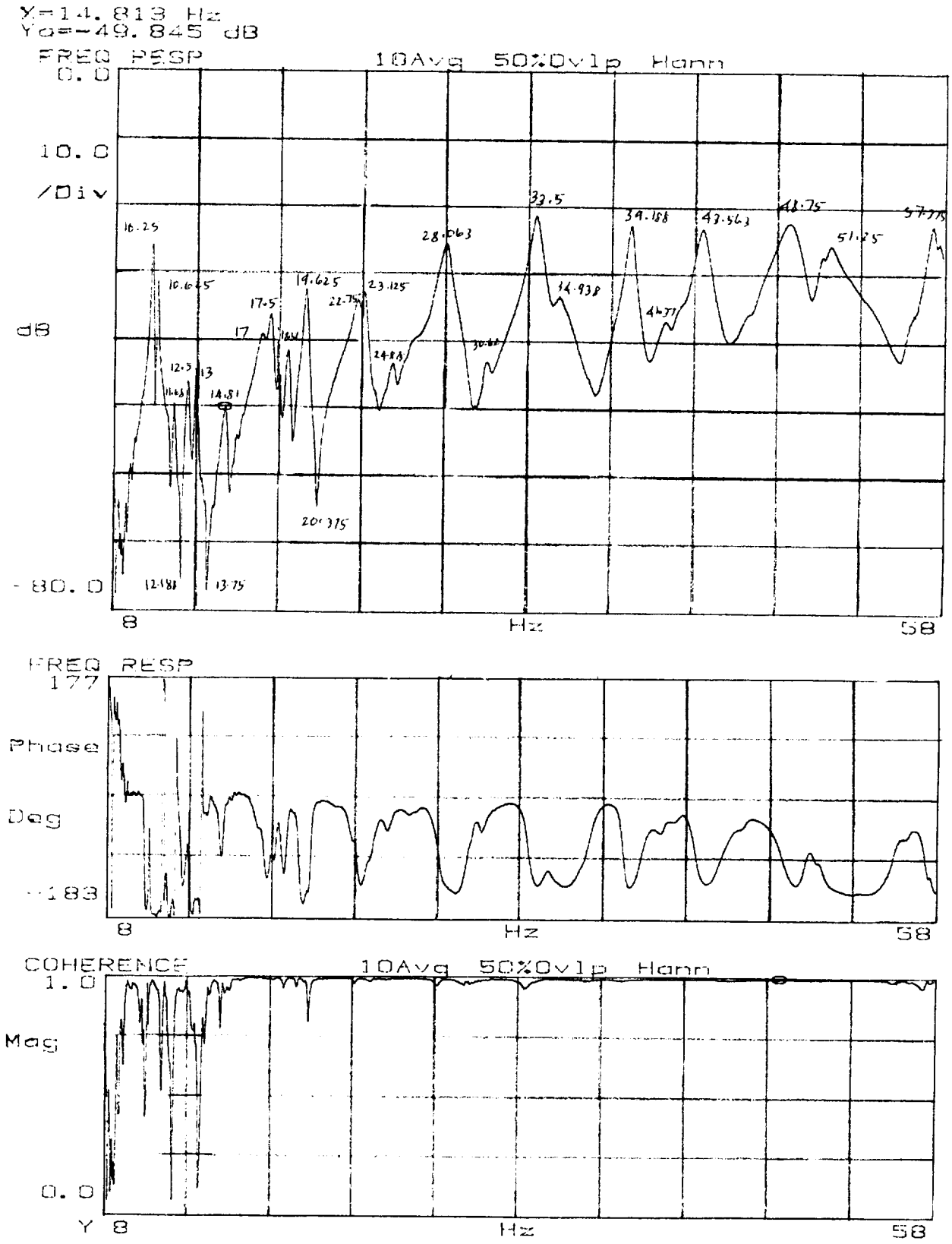

Figure 9: FRF (Bode plot) from the HP3562A analyzer.

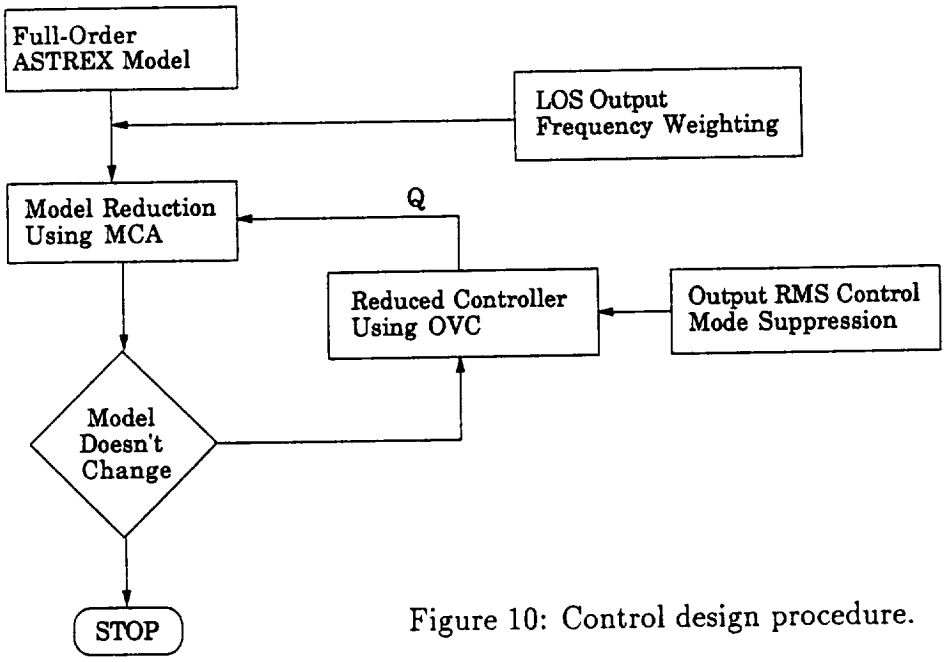

Figure 10: Control design procedure.

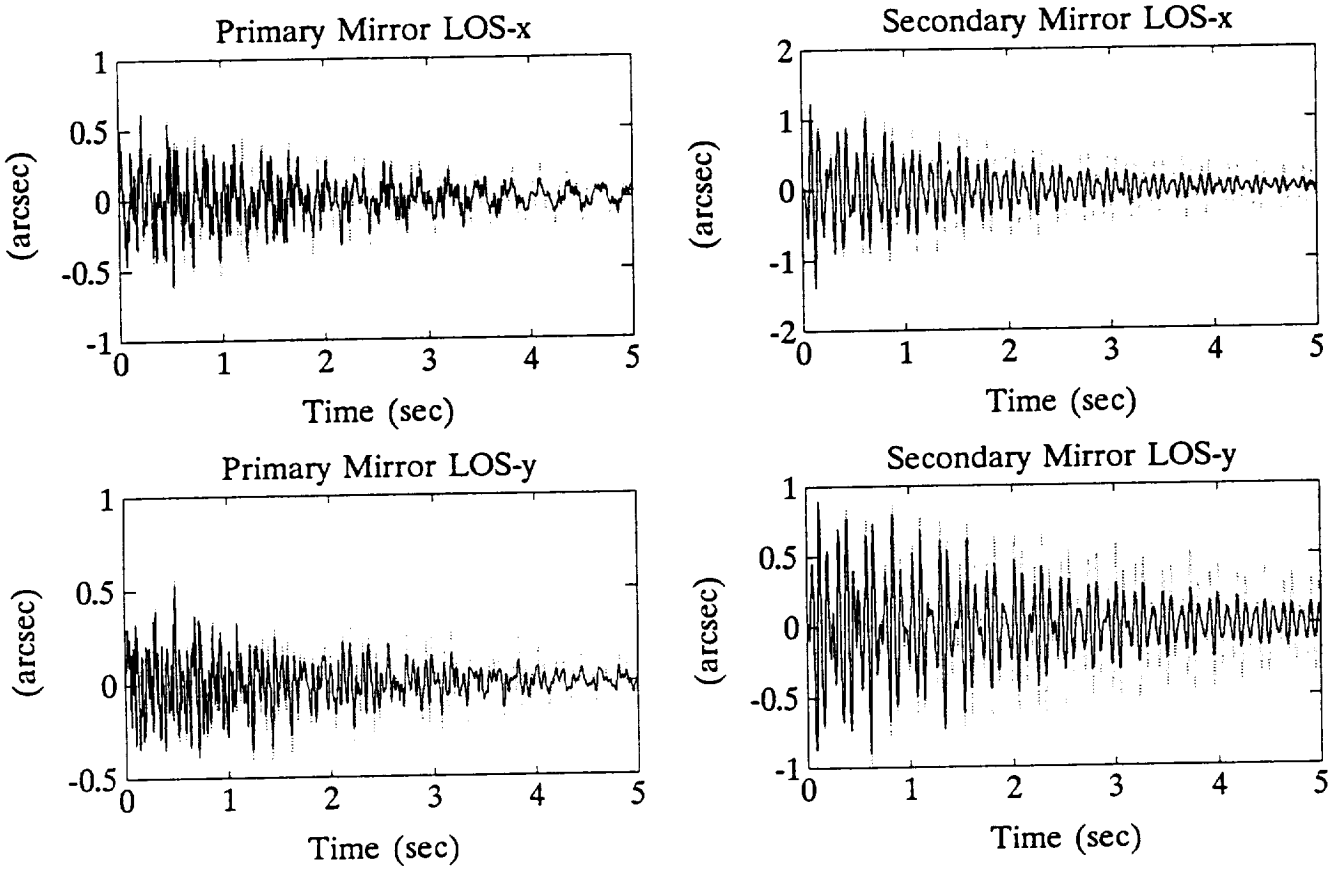

Figure 11: Pulse response to disturbance channel 6.